Accepted Manuscript

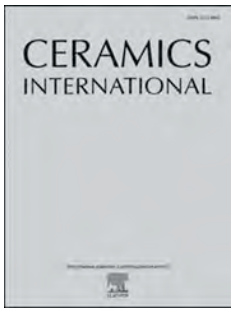

Anti-reductive characteristics and dielectric loss mechanisms of $Ba_2ZnSi_2O_7$ microwave dielectric ceramic

Zheng-Yu Zou, Kang Du, Xue-Kai Lan, Wen-Zhong Lu, Xiao-Chuan Wang, Xiao-Hong Wang, Wen Lei

PII: S0272-8842(19)31696-7

DOI: https://doi.org/10.1016/j.ceramint.2019.06.195

Reference: CERI 22004

To appear in: *Ceramics International*

Received Date: 16 May 2019

Revised Date: 18 June 2019

Accepted Date: 19 June 2019

Please cite this article as: Z.-Y. Zou, K. Du, X.-K. Lan, W.-Z. Lu, X.-C. Wang, X.-H. Wang, W. Lei, Anti-reductive characteristics and dielectric loss mechanisms of $Ba_2ZnSi_2O_7$ microwave dielectric ceramic, *Ceramics International* (2019), doi: https://doi.org/10.1016/j.ceramint.2019.06.195.

Anti-reductive characteristics and dielectric loss mechanisms of $Ba_2ZnSi_2O_7$ microwave dielectric ceramic

Zheng-Yu Zou[a,b], Kang Du[a,b], Xue-Kai Lan[a,b], Wen-Zhong Lu[a,b], Xiao-Chuan Wang[a,b], Xiao-Hong Wang[a,b], Wen Lei[a,b,*]

[a] School of Optical and Electronic Information, Huazhong University of Science and Technology, Wuhan 430074, P. R. China

[b] Key Lab of Functional Materials for Electronic Information (B), Ministry of Education, Wuhan 430074, P. R. China

Abstract

$Ba_2ZnSi_2O_7$ ceramic was prepared by conventional solid-state method and sintering under four different atmospheres (air, O_2, N_2, and N_2–1 vol% H_2). The $Ba_2ZnSi_2O_7$ ceramic exhibited a single phase under air, O_2, and, N_2, whereas two phases (including $BaSiO_3$ impurity) were observed under the N_2–1 vol% H_2 atmosphere due to Zn^{2+} evaporation. Dielectric loss was proportional to oxygen partial pressure due to the conduction mechanism of dominant holes. The $Ba_2ZnSi_2O_7$ ceramic exhibited good microwave dielectric properties (ε_r = 8.3, $Q\times f$ = 27200 GHz, τ_f = –41.5 ppm/°C) under the N_2–1 vol% H_2 atmosphere, making it a novel candidate with good anti-reductive characteristics for base metal electrode–multilayer ceramic capacitor applications.

* Corresponding author. Tel.: +86 27 8755 6493; fax: +86 27 8754 3134.
E-mail address: wenlei@mail.hust.edu.cn (W. Lei)

Keywords: Silicates; Electroceramics; Impedance spectroscopy; Anti-reductive characteristics

1. Introduction

Microwave dielectric ceramics are widely used as dielectric resonators (DR), antennas, filters, Multilayer ceramic capacitors (MLCCs), low temperature co-fired ceramics (LTCC) devices because of the excellent characteristics of high frequency, high speed transmission and wide passband [1,2,3]. MLCCs are important electronic components for the miniaturization of communication systems. The layers of MLCCs must increase to meet the technical parameters for high frequency, capacity, and precision. With the rapid pace of 5G development, the performance of ceramics and devices with microwave or millimeter-wave bands has attracted increasing research attention [4,5,6,7]. Low-permittivity (ε_r<15) microwave dielectric ceramics are generally used as dielectric layers [8]. However, the increase in the number of layers may promote the amount of internal electrodes, which is detrimental to industrial production. One of the main methods used to lower cost is the replacement of precious metals (Pt and Ag) with cheap base metal electrodes (BMEs; Cu and Ni) [9]. However, this measure encounters difficulties for base ceramics, including the following: (1) the sintering temperature must be lower than the melting point of BME (Ni: 1453 °C), (2) the base metals are sensitive to oxidation, and (3) the cofiring ceramics must be sintered in a reducing atmosphere [10].

Perovskite (Ba, Ca)(Zr, Ti)O_3 ceramics have been widely investigated as key materials for BME–MLCCs due to their high permittivity and low loss [9,11]. However, $BaTiO_3$-based ceramics contain various additives to enhance their anti-reductive

characteristics [12,13] and possess poor quality factor ($Q\times f$) in microwave frequency; these qualities are unsuitable for high-frequency and high-precision BME–MLCCs [14]. The complex perovskite-type ceramics $Ba(Zn_{1/3}Nb_{2/3})O_3$ and $Ba(Mg_{1/3}Nb_{2/3})O_3$ possess interesting microwave dielectric properties (ε_r = 33–39, $Q\times f$ = 63700–76700 GHz, τ_f = +30 to +33 ppm/°C), which are widely used to manufacture BME–MLCCs [15]. However, under the same capacitance, high-permittivity ceramics need fewer layers than low-permittivity ceramics. Decreased layer number may enhance errors in each layer, which can decrease precision. Meanwhile, low permittivity can reduce the reflection at the interface between air and dielectrics, minimize cross-coupling, and shorten the time for electronic signal transition [16]. Given that anti-reductive characteristics have not been extensively studied in low-permittivity microwave dielectric ceramics, novel materials should be developed for high-frequency and high-precision BME–MLCCs.

Low-permittivity (ε_r < 15) barium zinc silicate ceramics exhibit many interesting and attractive properties, such as the coexistence of weak ferroelectricity and low-permittivity microwave dielectric properties in $Ba_2Zn_{(1+x)}Si_2O_{(7+x)}$ ceramics [17,18]. The relative permittivity and stability against temperature can be improved by controlling the amount of Zn^{2+} ions and Ba/Si ratios for the barium zinc silicate ceramic system [18,19]. Unfortunately, the anti-reductive characteristics for barium zinc silicate ceramics sintered under a reducing atmosphere have not been investigated. Furthermore, the internal dielectric loss mechanism and the electrochemical properties remain unknown for barium zinc silicate ceramics. Therefore, we investigated the phase compositions, electrochemical performance, microwave dielectric properties, and anti-reductive characteristics of $Ba_2ZnSi_2O_7$ ceramic.

2. Experimental procedures

The solid-state method was used to prepare the $Ba_2ZnSi_2O_7$ ceramic by using analytical-grade $BaCO_3$ (99.8%, Shandong Boshan Chemical Reagent, China), ZnO (99.5%, Shanghai Shiyi Chemical Reagent, China), and SiO_2 (99.5%, Shanghai Hengxin Chemical Reagent, China) powders as raw materials. The raw materials with desirable stoichiometry were weighed and ball milled in a polyethylene jar for 5 h by using ZrO_2 balls with deionized water. The mixtures were calcined in air at 1100 °C for 3 h with a heating rate of 5 °C/min. The powders were then uniaxially pressed at 150 MPa, followed by sintering at a densification temperature between 1125 °C and 1200 °C for 3 h at a heating rate of 5 °C/min in air, oxygen, nitrogen, and reducing atmospheres (N_2–1 vol% H_2).

X-ray diffraction (XRD) data were obtained using an X-ray diffractometer (XRD-7000, Shimadzu, Kyoto, Japan) with CuKα radiation. The microstructures of the $Ba_2ZnSi_2O_7$ samples were observed by scanning electron microscopy (SEM; Sirion 200, the Netherlands). High-temperature impedance spectroscopy was employed using an Agilent 4294A impedance analyzer (Agilent, Santa Clara, USA) and VDMS-2000 measuring system (Partulab, Wuhan, China). The content of oxygen vacancies was identified by X-ray photoelectron spectroscopy (AXIS-ULTRA DLD-600W, Shimadzu, Kyoto, Japan). ε_r and the unloaded $Q\times f$ value were measured at approximately 12.5 GHz in the TE_{011} mode via the Hakki and Coleman method [20] by using a network analyzer (Agilent E8362B, Agilent Technologies, Santa Clara, USA) and parallel silver boards. τ_f in the temperature range of 25 °C–80 °C was calculated using Eq. (1):

$$\tau_f = \frac{1}{f(T_0)} \frac{[f(T_1) - f(T_0)]}{T_1 - T_0} \qquad (1)$$

where $f(T_1)$ and $f(T_0)$ represent the resonant frequency at T_1 (80 °C) and T_0 (25 °C), respectively.

3. Results and discussion

The XRD patterns of the $Ba_2ZnSi_2O_7$ ceramic sintered at 1200 °C under air, O_2, and N_2 and 1125 °C under the N_2–1 vol% H_2 atmosphere are shown in Fig. 1. The $Ba_2ZnSi_2O_7$ ceramic maintained a stable single-phase composition under air, O_2, and N_2 atmospheres. However, under the N_2–1 vol% H_2 atmosphere, the $Ba_2ZnSi_2O_7$ ceramic had a two-phase composition with $BaSiO_3$ and $Ba_2ZnSi_2O_7$.

Notably, $Ba_2ZnSi_2O_7$ had a higher Zn^{2+} content than $BaSiO_3$. Therefore, the transformation of phase compositions could be explained by Zn^{2+} evaporation. The $Ba_2ZnSi_2O_7$ ceramic lost Zn^{2+} under the N_2–1 vol% H_2 atmosphere and then converted to $BaSiO_3$. Ion vacancies were generated from Zn^{2+} evaporation, thereby influencing the phase structure and microwave dielectric properties, which are similar to the $La(Zn_{1/2}Ti_{1/2})O_3$ [21] and $Ba(Zn_{1/3}Ta_{2/3})O_3$ ceramics [8].

The SEM images of the thermally etched $Ba_2ZnSi_2O_7$ ceramic sintered under air and N_2–1 vol% H_2 atmosphere are presented in Fig. 2. A dense microstructure was observed in the $Ba_2ZnSi_2O_7$ ceramic sintered under both atmospheres. Notably, the densification temperature of the $Ba_2ZnSi_2O_7$ ceramic sintered under the N_2–1 vol% H_2 atmosphere was 75 °C lower than that of the specimen sintered in air. The high ion vacancy in the N_2–1 vol% H_2 atmosphere promoted the migration of substances, thereby lowering the densification temperature [22].

Impedance spectroscopy is an important method for analyzing electrochemical

properties and dielectric loss from conduction. Fig. 3(a) shows the impedance complex plane plots of $Ba_2ZnSi_2O_7$ ceramics at 600 °C–700 °C. Interceptive and suppressed arcs are presented for different testing temperatures. The arc or aiguille behind the semicircle in the low frequency remarkably determines whether the conduction is dominated by oxide ion [23]. However, an arc at low frequency cannot be determined due to the truncation of the arc. To further determine the type of conduction mechanisms, we showed the Z^* plots at 650 °C under different atmospheres (air, O_2, and N_2) in Fig. 3(b). With the increase in oxygen partial pressure, the conductivity increased gradually. This phenomenon indicated that the $Ba_2ZnSi_2O_7$ ceramic exhibited high-temperature p-type behavior.

Schottky-type defects, such as ion vacancies, may explain the p-type behavior [24]. The oxygen vacancies reacted with molecular oxygen to form holes in high oxygen partial pressure through the following equation [25]:

$$\frac{1}{2}O_2 + V_O^{\bullet\bullet} \rightarrow O_O^{\times} + 2h^{\bullet} \qquad (2)$$

The XRD results (Fig. 1) revealed that Zn^{2+} evaporation was accompanied with the formation of oxygen vacancies. Irreparable Zn^{2+} resulted in the formation of holes at high oxygen partial pressure, which led to the high-temperature p-type behavior. Thus, the Zn^{2+} vacancies played a major role in the p-type conduction of $Ba_2ZnSi_2O_7$ ceramics.

The electric modulus M^*, admittance Y^*, and impedance Z^* are alternative parameters to analyze electrochemical performance from the impedance data [26,27]. These variables represent the electrochemical properties from different physical

perspectives. In the electrically homogeneous phase, the imaginary part of impedance Z'' and electric modulus M'' can be described by the following equations [27,28]:

$$Z'' = R\left[\frac{\omega RC}{1+(\omega RC)^2}\right] \quad (3)$$

$$M'' = \frac{C_0}{C}\left[\frac{\omega RC}{1+(\omega RC)^2}\right] \quad (4)$$

In the Z'' and M'' plots, Debye-type peaks are caused by the response of different components, such as grain and grain boundary [25]. Maximum ω_{max} is generated at the Debye-type peak, and ω follows ω_{max}RC=1. Hence, at the Debye-type peaks, $M'' = \frac{C_0}{2C}$ reflects the minimum capacitance, and $Z'' = \frac{R}{2}$ represents the maximum resistance of components. The Z'' and M'' plots of the $Ba_2ZnSi_2O_7$ ceramic at 650 °C under air atmosphere are shown in Fig. 4. In general, the peaks of Z'' and M'' are located at the same frequency in the electrically homogeneous system [29]. However, the Z'' and M'' peaks of the $Ba_2ZnSi_2O_7$ ceramic correspond to different frequencies, and the magnitude of different frequencies is less than two orders, explaining the two electrical responses caused by the inter-grains and intra-grains [25]. The slight difference was insufficient to separate the arc in the Z^* plots completely, so deeply suppressed arcs are presented (Fig. 3).

Fig. 5(a) shows O-1s spectra and fitted Gaussian sub-peaks of the $Ba_2ZnSi_2O_7$ ceramic sintered under air, O_2, and N_2 atmospheres. The peaks at approximately 529.7, 530.8, and 531.7 eV are attributed to the oxygen in lattice (O_{lat}), oxygen vacancy (O_{vac}), and absorption of oxygen (O_{abs}) on the surface of the ceramics in the form of H_2O and/or O_2 [30,31,32]. The peak area ratios of oxygen vacancy (O_{vac}) to total oxygen (O_{lat}+O_{vac}+O_{abs}) under O_2, air, and N_2 sintering under atmospheres were 28.7%, 37.0%,

and 45.7%, respectively, for the $Ba_2ZnSi_2O_7$ ceramic, which were consistent with the impedance spectra. The oxygen vacancies combined with oxygen to form holes and were converted to the oxygen in lattice (Fig. 5(a)), illuminating that the content of oxygen vacancies and holes are directly related to oxygen partial pressure. Hence, the generation of holes by the combination of oxygen vacancies and oxygen was the main mechanism of high-temperature p-type conduction. In addition, oxygen vacancies bonded with silicon are subject to occur in silicates [33], which results in the reduction of the Si^{4+} valence state [34]. The Si-2p spectra and the fitted Gaussian sub-peaks of the $Ba_2ZnSi_2O_7$ ceramic sintered under air, O_2, and N_2 atmospheres in Fig. 5(b) confirmed the change of the Si^{4+} valence state. The peak area ratio of Si^{4+} were 20%, 34.9%, and 18.3% under air, O_2, and N_2 atmosphere, respectively, indicating that the valence changes of silicon compensated the valence state balance with the holes created from oxygen vacancies [35]. In addition, oxygen vacancies led to the increase in the tilting (and/or distortion) of tetrahedrons and structural instability, which resulted in incommensurate structures and ferroelectricity [32,36,37].

Table 1 shows the phase compositions, sintering atmosphere, relative density and microwave dielectric properties of $Ba_2ZnSi_2O_7$ ceramic sintered at 1125–1200 °C for 3 h. The high relative density proves that ceramics can maintain dense structure under four atmospheres, which is consistent with the SEM results. The ε_r of $Ba_2ZnSi_2O_7$ ceramic was approximately 8 under four atmospheres. According to the impedance spectrum analysis, the p-type behavior of the $Ba_2ZnSi_2O_7$ ceramic generated more holes under O_2 atmosphere. The increased hole migration enhanced the loss, resulting in the reduction of $Q\times f$ value. Therefore, the variation trend of $Q\times f$ value was opposite to that

of oxygen partial pressure in the $Ba_2ZnSi_2O_7$ ceramic. However, the $Q\times f$ value under the N_2-1 vol% H_2 atmosphere was reduced slightly compared with that under the N_2 atmosphere due to the negative effect of $BaSiO_3$ second phase with lower $Q\times f$ value (6600 GHz) in the former [38].

The Zn^{2+} content may remarkably deteriorate the τ_f value in $Ba_2Zn_{(1+x)}Si_2O_{(7+x)}$ ceramic systems [18]. High oxygen partial pressure prevented Zn^{2+} from evaporation. Hence, the τ_f value increased along the negative direction. The second phase $BaSiO_3$ (ε_r=11.1, $Q\times f$=6600 GHz, τ_f=–35.4 ppm/°C) appeared in the $Ba_2ZnSi_2O_7$ ceramic under the N_2–1 vol% H_2 atmosphere, which improved the τ_f value to –41.5 ppm/°C. This phenomenon could be explained by the τ_f value of the following mixing rule of multi-phase ceramics:

$$\tau_{\mathrm{f}} = \sum_{i=1}^{k} v_{\mathrm{i}} \tau_{\mathrm{fi}} \qquad (5)$$

where v_{i} and τ_{fi} are the volume fraction and temperature coefficient of the resonant frequency of the *i*th phase, respectively.

4. Conclusions

Low-permittivity $Ba_2ZnSi_2O_7$ microwave dielectric ceramic was prepared via the conventional solid-state method. The $Ba_2ZnSi_2O_7$ ceramic presented a stable phase structure under air, O_2, and N_2 atmospheres. However, Zn^{2+} evaporation in the N_2–1 vol% H_2 atmosphere may remarkably increase ion vacancies and deteriorate the stability of the phase structure, resulting in the coexistence of $BaSiO_3$ and $Ba_2ZnSi_2O_7$ in two phases. The volatilization of Zn^{2+} facilitated the appearance of Schottky-type defects accompanied with the formation of oxygen vacancies. The $Ba_2ZnSi_2O_7$ ceramic

presented high-temperature p-type conduction because Zn^{2+} could not be compensated during cooling. Holes appeared from the occupation of oxygen vacancies by oxygen at high oxygen partial pressure. On the basis of the p-type conduction characteristic of the $Ba_2ZnSi_2O_7$ ceramic, the dielectric loss was directly proportional to the oxygen partial pressure. Given the dominance of hole conduction, the $Ba_2ZnSi_2O_7$ ceramic presented good microwave dielectric properties (ε_r = 8.3, $Q\times f$ = 27200 GHz, τ_f = –41.5 ppm/°C) under the N_2–1 vol% H_2 atmosphere. Therefore, the $Ba_2ZnSi_2O_7$ ceramic possessed good anti-reductive characteristics for high-frequency and high-precision BME–MLCCs.

Acknowledgements

This work was supported by the National Natural Science Foundation of China (NSFC-51572093, 51772107, and 61771215), the Equipment Development Department of China (1807WM0004), and the Major Programs of Technical Innovation in Hubei Province of China (2018AAA039). The authors are grateful to the Analytical and Testing Center, Huazhong University of Science and Technology, for XPS analyses.

References

[1] I.M. Reaney, D. Iddles, Microwave dielectric ceramics for resonators and filters in mobile phone network, J. Am. Ceram. Soc. 89 (2006) 2063-2072.

[2] D. Zhou, D. Guo, W.B. Li, L.X. Pang, X. Yao, D.W. Wang, I.M. Reaney, Novel temperature stable high-ε r microwave dielectrics in the Bi_2O_3–TiO_2–V_2O_5 system. J. Mate. Chem. C. 4 (2016) 5357-5362.

[3] D. Zhou, L.X. Pang, D.W. Wang, C. Li, B.B Jin, I.M. Reaney, High permittivity and low loss microwave dielectrics suitable for 5G resonators and low temperature co-fired ceramic architecture. J. Mate. Chem. C. 5 (2017) 10094-10098.

[4] L.X. Pang, D. Zhou, Modification of $NdNbO_4$ microwave dielectric ceramic by Bi substitutions, J. Am. Ceram. Soc. 102 (2019) 2278-2282.

[5] H.F. Zhou, X.H. Tan, J. Huang, N. Wang, G.C. Fan, X.L. Chen, Phase structure, sintering behavior and adjustable microwave dielectric properties of $Mg_{1-x}Li_{2x}Ti_xO_{1+2x}$ solid solution ceramics, J. Alloy. Compd. 96 (2017) 1255-1259.

[6] L.C Han, S.H. Ding, T.X. Song, L. Huang, X.Y. Zhang, Z. Xiong, ZBAS on the structure and dielectric property of $BaAl_2Si_2O_8$, J. Inorg. Mater. 33 (2018) 883-888.

[7] Y.A. Huang, B. Lu, Y.X. Zou, D.D. Li, Y.B. Yao, T. Tao, B. Liang, S.G. Liang, Grain size effect on dielectric, piezoelectric and ferroelectric property of $BaTiO_3$ ceramics with fine grains, J. Inorg. Mater. 33 (2018) 767-772.

[8] G.L. Brennecka, J.F. Ihlefeld, J.P. Maria, B.A. Tuttle, P.G. Clem, Processing technologies for high-permittivity thin films in capacitor applications, J. Am. Ceram. Soc. 93 (2010) 3935-3954.

[9] R.I. Scott, M. Thomas, C. Hampson, Development of low cost, high performance $Ba(Zn_{1/3}Nb_{2/3}O_3)$ based materials for microwave resonator applications, J. Eur. Ceram. Soc. 23 (2003) 2467-2471.

[10] J.S. Kim, J.W. Kim, C.I. Cheon, Y.S. Kim, S. Nahm, J.D. Byun, Effect of chemical element doping and sintering atmosphere on the microwave dielectric properties of barium zinc tantalates, J. Eur. Ceram. Soc. 21 (2001) 2599-2604.

[11] S. Wang, H. He, H. Su, Effect of synthesized $BaTiO_3$ doping on the dielectric properties of ultra temperature-stable ceramics, J. Mater. Sci.: Mater. Electron. 23 (2012) 1875–1880.

[12] H. Kishi, Y. Mizuno, H. Chazono, Base-metal electrode-multilayer ceramic capacitors: past, present and future perspectives, Jpn. J. Appl. Phys. 42 (2003) 1-15.

[13] D.F.K. Hennings, Dielectric materials for sintering in reducing atmospheres, J. Eur. Ceram. Soc. 21 (2001) 1637-1642.

[14] Y. Wang, K.K. Miao, W.J. Wang, Y. Qin, Fabrication of lanthanum doped $BaTiO_3$ fine-grained ceramics with a high dielectric constant and temperature-stable dielectric properties using hydro-phase method at atmospheric pressure, J. Eur. Ceram. Soc. 37 (2017) 2385-2390.

[15] A. Veres, S. Marinel, F. Roulland, Dielectric properties of $Ba(Mg,Zn)_{1/3}Nb_{2/3}O_3$ and effect of B_2O_3 and LiF addition, J. Eur. Ceram. Soc. 25 (2005) 2759-2762.

[16] W. Lei, W.Z. Lu, X.H. Wang, F. Liang, J. Wang, Phase Composition and microwave dielectric properties of $ZnAl_2O_4$–Co_2TiO_4 low-permittivity ceramics with high quality factor, J. Am. Ceram. Soc. 94 (2011) 20-23.

[17] Z.Y. Zou, X.K. Lan, W.Z. Lu, G.F. Fan, X.H. Wang, X.C. Wang, P. Fu, W. Lei, Novel high Curie temperature $Ba_2ZnSi_2O_7$ ferroelectrics with low-permittivity microwave dielectric properties, Ceram. Int. 42 (2016) 16387-16391.

[18] Z. Y. Zou, Z. H. Chen, X. K. Lan, W. Z. Lu, U. Burhan, X. H. Wang, W. Lei, Weak ferroelectricity and low-permittivity microwave dielectric properties of $Ba_2Zn_{(1+x)}Si_2O_{(7+x)}$ ceramics, J. Eur. Ceram. Soc. 37 (2017) 3065-3071.

[19] W. Lei, Z.Y. Zou, Z.H. Chen, B. Ullah, A. Zeb, X.K. Lan, W.Z. Lu, G.F. Fan, X.H. Wang, X.C. Wang, Controllable τ_f value of barium silicate microwave dielectric ceramics with different Ba/Si ratios, J. Am. Ceram. Soc. 101 (2018) 25–30.

[20] B.W. Hakki, P.D. Coleman, A dielectric resonator method of measuring inductive capacities in the millimeter range, IRE Trans. Microw. Theory Technol. 8 (1960) 402-410.

[21] S.Y. Cho, M.K. Seo, K.S. Hong, S.J. Park, Influence of ZnO evaporation on the microwave dielectric properties of $La(Zn_{1/2}Ti_{1/2})O_3$, Mater. Res. Bull. 32 (1997) 725-735.

[22] X.W. Liu, K. Zhou, L. Wang, B. Wang, Y.D. Li, Oxygen vacancy clusters promoting reducibility and activity of ceria nanorods, J. Am. Ceram. Soc. 131 (2009) 3140-3141.

[23] M. Li, M.J. Pietrowski, R.De. Souza, H. Zhang, I.M. Reaney, S. N. Cook, J. A. Kilner, D.C. Sinclair, A family of oxide ion conductors based on the ferroelectric perovskite $Na_{0.5}Bi_{0.5}TiO_3$, Nat. Mater. 13 (2014) 31.

[24] P. Erhart, K. Albe, Modeling the electrical conductivity in $BaTiO_3$ on the basis of

first-principles calculations, J. Appl. Phys. 104 (2008) 044315.

[25] Z.P. Gao, L.F. Wu, C.J. Lu, W. Gu, T. Zhang, G.M. Liu, Q.H. Xie, M. Li, The anisotropic conductivity of ferroelectric $La_2Ti_2O_7$ ceramics, J. Eur. Ceram. Soc. 37 (2017) 137-143.

[26] E. Barsoukov, J.R. Macdonald, Impedance spectroscopy: theory, experiment and applications, John Wiley & Sons, New Jersey,2005.

[27] I. Hodge, M. Ingram, A.R. West, Impedance and modulus spectroscopy of polycrystalline solid electrolytes, J. Electroanal. Chem. Interfacial Electrochem. 74 (1976) 125–143.

[28] J. Irvine, D.C. Sinclair, A.R. West, Electroceramics: characterization by impedance spectroscopy, Adv. Mater. 2 (1990) 132–138.

[29] M. Li, L. Li, J. Zang, D.C. Sinclair, Donor-doping and reduced leakage current in Nb-doped $Na_{0.5}Bi_{0.5}TiO_3$, Appl. Phys. Lett. 106 (2015) 102904.

[30] K. Kim, S.Y. Park, K.H. Lim, C. Shin, J.M. Myoung, Y.S. Kim, Low temperature and solution-processed Na-doped zinc oxide transparent thin film transistors with reliable electrical performance using methanol developing and surface engineering, J. Mater. Chem. 22 (2012) 23120-23128.

[31] Y. Jung, W. Yang, C.Y. Koo, K. Song, J. Moon, High performance and high stability low temperature aqueous solution-derived Li–Zr co-doped ZnO thin film transistors, J. Mater. Chem. 22 (2012) 5390-5397.

[32] B. Ullah, W. Lei, X.H. Wang, G.F. Fan, X.C. Wang, W.Z. Lu, Dielectric and ferroelectric behavior of an incipient ferroelectric $Sr_{(1-3x/2)}Ce_xTiO_3$ novel solid solution,

RSC Adv. 6 (2016) 91679-91688.

[33] L.R.C. Fonseca, A.L. Xavier, M. Ribeiro, C. Driemeier, I.J.R. Baumvol, Hydrogen trapping in oxygen-deficient hafnium silicates, J. Appl. Phys. 102 (2007) 044108.

[34] M.Y. Bashouti, K. Sardashti, J. Ristein, S.H. Christiansen, Early stages of oxide growth in H-terminated silicon nanowires: determination of kinetic behavior and activation energy, Phys. Chem. Chem. Phys. 14 (2012) 11877-11881.

[35]J.D. Zang, M. Li, D.C. Sinclair, W. Jo, J. Rödel, Impedance spectroscopy of $(Bi_{1/2}Na_{1/2})TiO_3$–$BaTiO_3$ ceramics modified with $(K_{0.5}Na_{0.5})NbO_3$, J. Am. Ceram. Soc. 97 (2014) 1523-1529.

[36] R.D. Shannon, Dielectric polarizabilities of ions in oxides and fluorides, J. Appl. Phys. 73 (1993) 348-366.

[37] H.Taniguchi, A. Kuwabara, J. Kim, Y.H. Kim, H. Moriwake, S. Kim, T. Hoshiyama, S. Mori, M. Takata, H. Hosono, Y. Inaguma, M. Itoh, Ferroelectricity driven by twisting of silicate tetradral chains, Angew. Chem. Int. Ed. 52 (2013) 8088-8092.

[38] H.Z. Zuo, X.L. Tang, H. Guo, Q.G. Wang, C.L. Dai, H.W. Zhang, H. Su, Effects of $BaCu(B_2O_5)$ addition on microwave dielectric properties of Li_2TiO_3 ceramics for LTCC applications, Ceram. Int. 43 (2017) 13913-13917.

Figure Captions

Fig. 1. The XRD patterns of $Ba_2ZnSi_2O_7$ ceramic sintered at (a)1200 °C, air; (b) 1200 °C, O_2; (c) 1200 °C, N_2 and (d) 1125 °C, N_2-1 vol%H_2 sintering atmospheres.

Fig. 2. SEM images of the thermally etched $Ba_2ZnSi_2O_7$ ceramic sintered in different atmosphere: (a) air, 1200 °C; (b) N_2-1 vol%H_2, 1125 °C.

Fig. 3. (a) Impedance complex plane plots of $Ba_2ZnSi_2O_7$ ceramic at 600-700 °C, (b) Comparison of Z^* plots for $Ba_2ZnSi_2O_7$ ceramics at 650 °C under air, oxygen and nitrogen atmospheres.

Fig. 4. The Z″ and M″ plots of $Ba_2ZnSi_2O_7$ ceramic at 650 °C under air atmosphere.

Fig. 5. (a)O-1s (b)Si-2p spectra and fitted Gaussian sub-peaks of the $Ba_2ZnSi_2O_7$ ceramic under air, O_2 and N_2 atmospheres.

Table

Table 1 The sintering atmosphere, phase compositions, relative density and microwave dielectric properties of $Ba_2ZnSi_2O_7$ ceramic

Sintering atmosphere	ε_r	$Q\times f$ (GHz)	τ_f (ppm/°C)	ρ_r (%)	Phase compositions
Air	8.09	26600	–51.4	96.4	$Ba_2ZnSi_2O_7$
O_2	8.30	23200	–60.1	95.7	$Ba_2ZnSi_2O_7$
N_2	8.59	28300	–52.4	95.2	$Ba_2ZnSi_2O_7$
N_2-1 vol%H_2	8.30	27200	–41.5	95.6	$Ba_2ZnSi_2O_7$+$BaSiO_3$

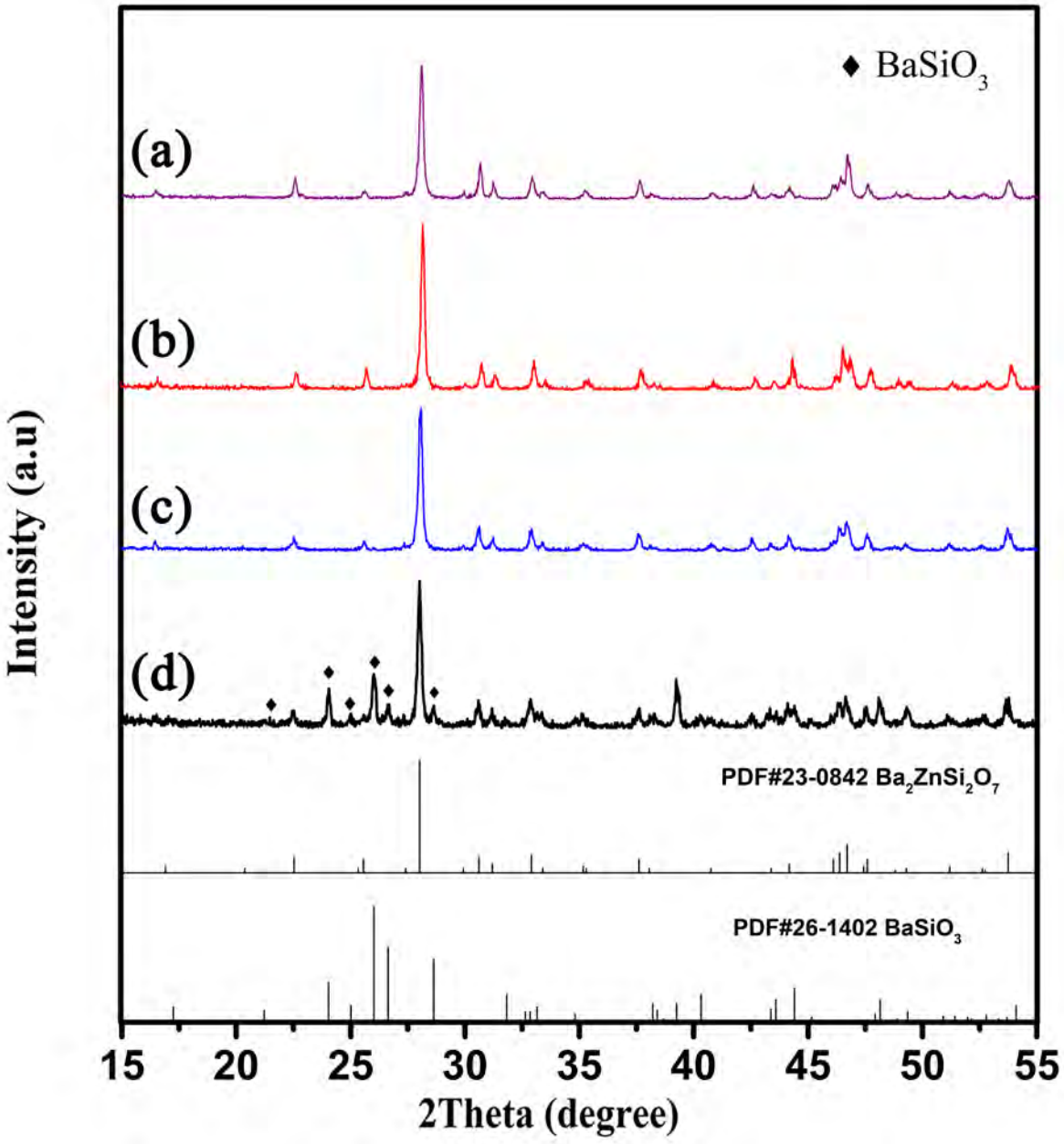
♦ BaSiO3
(a)
(b)
(c)
(d)
PDF#23-0842 Ba2ZnSi2O7
PDF#26-1402 BaSiO3
Intensity (a.u)
15
20
25
30
35
40
45
50
55
2Theta (degree)

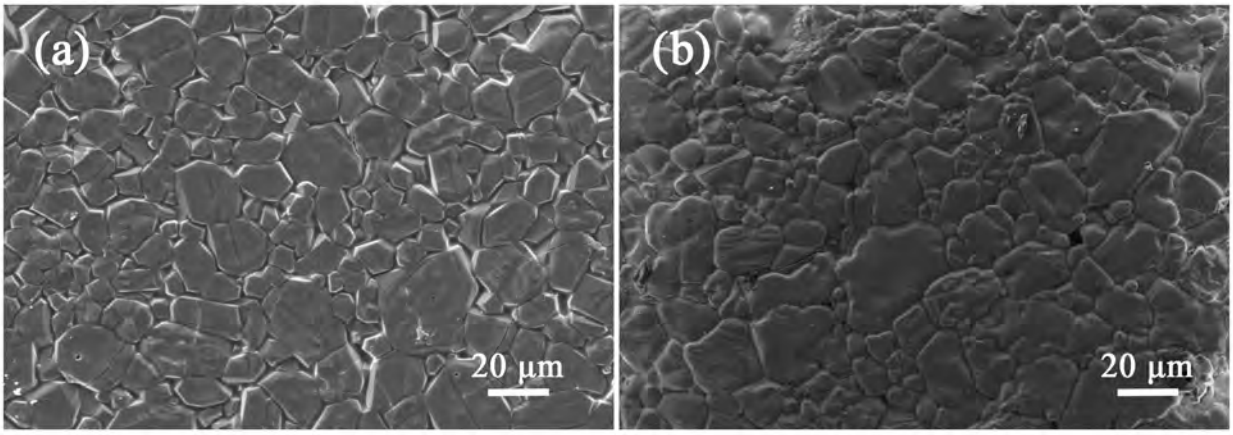

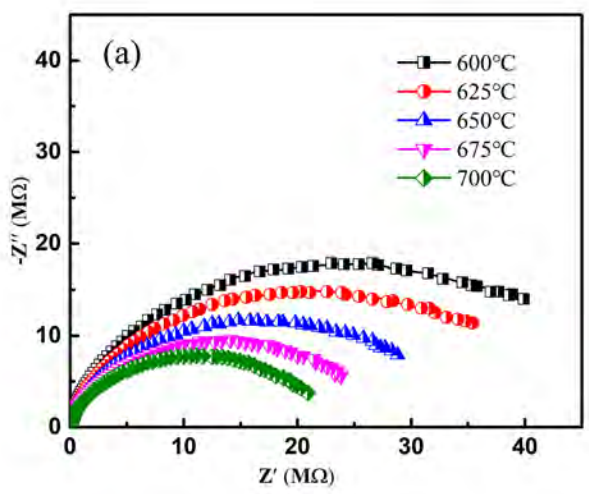

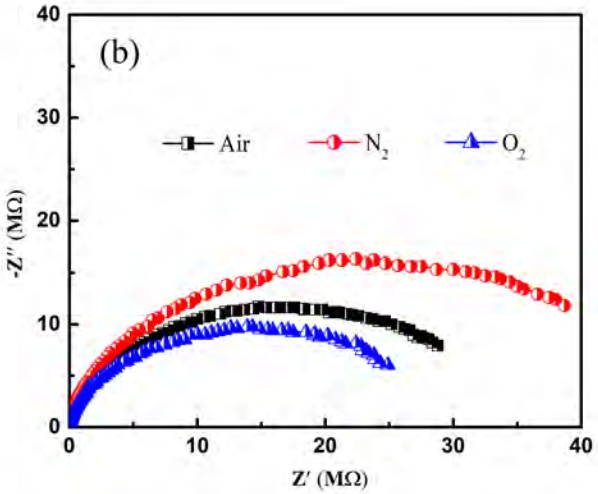

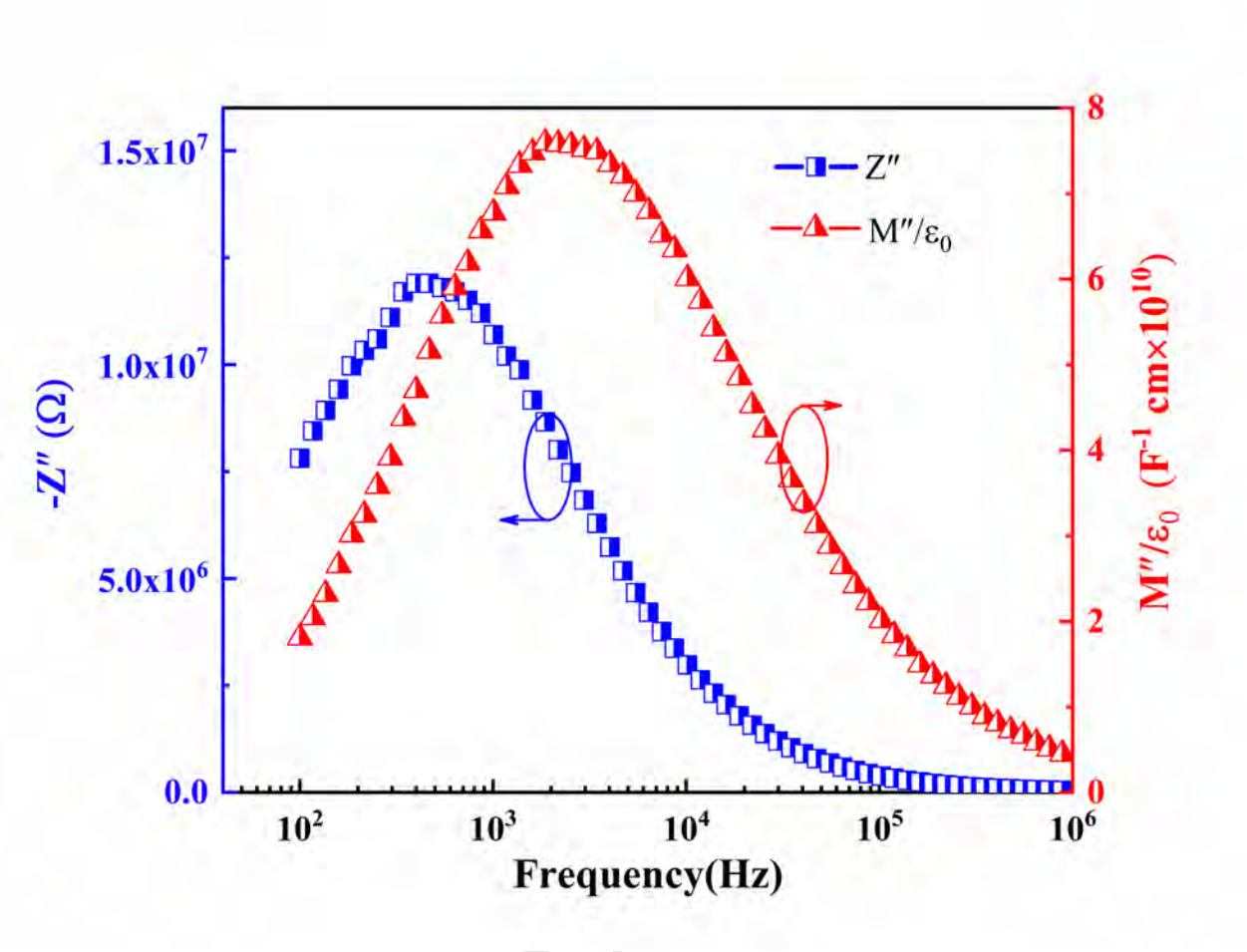
1.5x10^7
1.0x10^7
5.0x10^6
0.0
-Z″ (Ω)
8
6
4
2
0
M″/ε0 (F^-1 cm×10^10)
Z″
M″/ε0
10^2
10^3
10^4
10^5
10^6
Frequency(Hz)